Moustafa et al | Article 9480
J Pure Appl Microbiol. 2024;18(3):1969-1983. doi: 10.22207/JPAM.18.3.47
Received: 20 April 2024 | Accepted: 20 June 2024
Published Online: 29 August 2024

P-ISSN: 0973-7510; E-ISSN: 2581-690X

RESEARCH ARTICLE OPEN ACCESS

Preparing and Assessment of Biocidal La Nano-complex Treated Filter Capacity against Isolated Microbes from Air Conditioning Systems in COVID-19 Rehabilitation Rooms

Shaima M. N. Moustafa[1]*, Tarak A. Yousef[2,3] and Rania H. Taha[4,5]

[1]Biology Department, College of Science, Jouf University, P.O. Box: 2014, Sakaka, Saudi Arabia.
[2]College of Science, Chemistry Department, Imam Mohammad Ibn Saud Islamic University, Riyadh 11623, Saudi Arabia.
[3]Department of Toxic and Narcotic Drug, Forensic Medicine, Mansoura Laboratory, Medicolegal Organization, Ministry of Justice, Cairo 11435, Egypt.
[4]Department of Chemistry, Faculty of Science (Girls), Al-Azhar University, Yousef Abbas Str., Nasr City, Cairo, Egypt.
[5]Chemistry Department, College of Science, Jouf University, P.O. Box: 2014, Sakaka, Saudi Arabia.

Abstract

Mucormycosis is a severe fungal infection which mainly caused by filamentous fungi of the *Absidia* sp., *Rhizopus* sp., *Cunninghamella* sp, *Mucor* sp., and *Rhizomucor* sp. Moreover, the pandemic of the SARS-CoV-2 virus expands the need to interfere with spread of the airborne respiratory infections. Accordingly, developing cutting-edge solutions to restrict and/or prevent air contamination by infectious microbes are very warranted. The current work aims to prepare biocidal La-nano complex treated filters and assess their anti-fungal capacity against 20 *Rhizopus oryzae*, 10 *Candida albicans*, and 11 *Aspergillus fumigatus.* These fungi were isolated from the inside parts of the air conditioning systems in the rehabilitation rooms for COVID-19 patients. The obtained results demonstrated that the prepared were able to significantly decrease the invading microbes and eradicate *Rhizopus, Aspergillus, Mucor, Candida albicans* isolates at 0.64 mg/ml concentration. DFT study compares the electronic properties and reactivity of a ligand in its uncoordinated form with its lanthanum complex. The ligand exhibits lower binding energy, ionization potential, electron affinity, absolute electronegativity, and chemical potential when coordinated with lanthanum. In contrast, the lanthanum complex has a smaller energy gap, absolute hardness, and global softness.

Keywords: Mucormycosis, DFT, COVID-19, Biocide La-nano Complex Treated Filters

***Correspondence:** shymaa.nabil@ju.edu.sa

Citation: Moustafa SMN, Yousef TA, Taha RH. Preparing and Assessment of Biocidal La Nano-complex Treated Filter Capacity against Isolated Microbes from Air Conditioning Systems in COVID-19 Rehabilitation Rooms. *J Pure Appl Microbiol.* 2024;18(3):1969-1983. doi: 10.22207/JPAM.18.3.47

INTRODUCTION

A new, opportunistic, life-threatening mycosis that affects both industrialized and developing countries worldwide is known as mucormycosis.[1] The fungi of order Mucorales, class Zygomycetes, genus *Mucor, Rhizopus, Cunninghamella*, and *Absidia* are the causative agents of this illness.[2-4] These fungi are distributed throughout the nature where they can be found in the ground, air, and water that has been tainted by pollutants, rotting fruits and vegetables, stored grains, groundnuts, bread, rice, wheat, and barley, as well as in dung and compost.[3] The nose, sinuses, and eyes are the main targets of these fungi before their dissemination into the brain. In addition, the causative agents of mucormycosis favor the elastic lamina of both the big and small arteries leading to bleeding, infarction, and thrombosis.[4] The illness can strike suddenly or spread rapidly causing epidemic, killing large numbers of vulnerable people, especially those with impaired immune systems.[2,4]

Of interest, Zygomycosis has been considered a new obstacle in the battle against the COVID-19 threat.[5] A variety of conditions, including HIV/AIDS, continuous use of hydrocortisone and a wide range of antibacterial antibiotics, acidosis, malnutrition, debility, leukemia, stem cell recipient, severe burns, emaciation, diabetes mellitus, etc. are associated with Zygomycosis.[6-9]

Of note, the majority of people with mucormycosis were either chronic diabetics or had received unreasonable corticosteroid treatment.[6-9] Humans being in close contact with pathogenic fungal species in the environment can develop mucormycosis. The skin infection might occur if a pathogenic fungal species comes into the skin via a cut, burn, or another type of skin injury.[10]

There is currently no vaccine available to mucormycosis, however, some therapies are in use to decrease the disease incidence risk in people with impaired immune systems.[10]

The typical person breathes about 16 kilograms of air each day.[11] Influenza, common cold, bronchitis, headaches, eye pain, coughing, and dizziness all are associated with inhaling polluted air. The inhaled airborne spores can transmit to the lungs or nasal cavities, and toxins production including particularly aggressive substances can also take place.

Indoor activities produced moisture which supports the growth of molds whether it is cold, wet, or hot and muggy summer times. Mold grows on many different surfaces, including clothes, books, toys, CDs, and even walls, and has the power to turn treasured possessions into dingy relics. While mold infiltration cannot be controlled, exposure of the equipment to molds can be decreased by the use of air filtration systems, isolation procedures, and environmental protection measures.[12] Since filters have the potential to act as a reservoir for contaminants in the indoor environment, the possibility of using silver nanoparticles in filter meshes has been investigated in several studies.[13-15] Silver nanoparticles were incorporated into a nanofibrous air filter to provide an antimicrobial effect.[16] Gram (+ve) and Gram (-ve) bacteria on the filters are less likely to survive when silver nanoparticles are present. No growth was seen over 24 hours, suggesting that the action was bacteriostatic rather than bactericidal.

In this study, we thought to follow the currently applied strategies of preparing biocidal filters. We examined the capacity of the prepared La nano-complex treated filters to restrict/prevent the spread of airborne microbes.

MATERIALS AND METHODS

Materials

The purity of all the substances used in the study was at the highest level. (BDH) produced pure organic solvents like C_2H_5OH and Dimethyl Formamide (DMF). Additionally, 5-bromo-salicylaldehyde (Sigma), *O*-phenylenediamine (Aldrich), and La $(NO_3)_3.6H_2O$ (Merck) were used.

Instruments

Using a 600 MHZ spectrometer, the 1H and 13C nuclear magnetic resonance spectra were captured in DMSO-d6. Dimethylformamide (DMF) was used as the solvent at room temperature, and the molar conductance was measured using a JEN WAY 4510 conductivity meter at Jouf University. A Perkin-Elmer 437 IR spectrometer was used to record the IR spectra of KBr discs between 400 and

4000 cm^{-1}. The average nano complex diameter was calculated using ImageJ software by randomly selecting 100 photos from each sample's Scan Electron Microscope images, (SEM; version 1.4.3).

Free ligand synthesis

A 2.01 g, 20 mmol, *O*-phenylenediamine (0.54 g, 10 mmol) heated solution was added to a heated and stirred 30 ml of 5-bromosalicylaldehyde in 100% C_2H_5OH. The stirred compounds were refluxed for two hours and then allowed to cool before the precipitate was filtered out and collected. The ligand was made using M. P; 240; yield (90.3 percent) as has been reported in an earlier study.[17]

Nano La complex synthesis

Free ligand (0.0025 mol) and (0.005 mol) of $La(NO_3)_3.6H_2O$ (1:2 molar ratio) were mixed to produce the nano La complex. The substances were crushed in a mortar at room temperature and were left some time to set up. The La-nano complex was crystallized as a light brown substance. The nano complex is a stable powder that dissolves in DMSO and DMF but not in other solvents.

Coating sterilized filter with La-nano-complex

A sterilized filter was cut into small pieces of 0.5 cm × 2 cm each, and equal volumes (100 ml) of 3% carboxymethylcellulose (CMC) and La-nano-complex (0.64 mg/ml) were mixed. The sterilized filters were then sprayed and coated with this mixture. After being prepared, the filter pieces were left overnight in an uncovered petri dish to dry at room temperature. The coating procedure was carried out in the dark at room temperature allowing the coating step to be carried out for 15, 30, and 60 minutes.[18]

Isolation and characterization of the growing fungal species

The filters of the air conditioners in the COVID-19 rehabilitation rooms were removed and cleaned 3 times with sterile type 3 water. Each filter was dried, and filter fragments of (1 × 3 cm) were prepared. These fragments were allowed to be placed in 330 ml sanitized water bottles. The Potato Dextrose Agar (PDA) media was prepared by adding 10 ml of Rose Bengal with PDA to 5 ml sterile ddH_2O. The filter fragments were individually placed on a sterile plate and the mixture was incubated at 26°C for five days.[19]

We followed described methods by Ainsworth *et al*. to grow and characterize the isolated grown microbes using the digital camera Motic microscope and the scanning electron microscope (the electronic microscopy unit, King Saud University, KSA).

Antifungal activity

The agar-well diffusion technique was used to assess the antifungal activity of the prepared La-nano complexes.[6] Inoculum stock for each isolate was prepared in PDB. On the surfaces of separate agar plates, each isolate was inoculated and a cork borer was used to create wells with a 0.2 mm diameter. 100 µl of the prepared nano La complexes in four different concentrations (0.32, 0.64, 1.28, and 2.56 mg/ml) were poured into the wells. The petri dishes were incubated at 26°C for 5 days. The antifungal activity was calculated based on the diameter of the inhibitory zone. Every experiment was carried out twice.[20-21]

DFT studies

We performed cluster calculations using the $DMoL^3$ program[22] in the Materials Studio package,[23] which is designed for the realization of large-scale density functional theory (DFT) calculations. DFT semi-core pseudopods calculations (dspp) were performed with the double numerical basis sets plus polarization functional (DNP). The DNP basis sets are of comparable quality to 6-31G Gaussian basis sets.[24] Kessi and Delley showed that the DNP basis sets are more accurate than Gaussian basis sets of the same size.[25] The RPBE functional[26] is so far the best exchange–correlation functional,[27] based on the generalized gradient approximation (GGA), and is employed to take account of the exchange and correlation effects of electrons. The geometric optimization was performed without any symmetry restriction.

RESULTS AND DISCUSSION

In the current study, the growing microbes in the filters of the air conditioning systems were visually and microscopically investigated and

purely isolated on PDA media. They were identified by analyzing the morphological characteristics (Figure 1) and nucleotide sequence of the ITS, calmodulin gene, and TEF-1α gene. Of the 5 different samples, 4 species were defined to belong to 5 genera. The fungi prevalence was *Rhizopus oryze* (37.35%), *Mucor irregularis* (1%), *Aspergillus niger* (20.4%), *Aspergillus fumigatus* (9.16%), and *Candida glabrata* (2.79%) (Table 1). This reflects similar risk ratios to those reported in COVID-19 coinfected patients. The morphological features of the isolated fungi (*Aspergillus fumigatus*, *Aspergillus niger*, *Candida glabrata*, *Rhizopus oryze,* and *Mucor irregularis)* are seen in Figure 1. SARS-CoV-2 and fungus infections have been documented among several nations like Germany, Brazil, the United States, India, China, France, Colombia, Argentina, Spain, Portugal, Austria, and Qatar.

Previous reports indicated that COVID-19 patients who have fungal co-infections showed a greater possibility of death especially, if they have additional underlying illnesses like hypertension, diabetes mellitus, oncological illnesses, kidney, heart, and liver problems (Table 2).[26,28,29]

Table 1. Number and percentages of fungal isolates from different filters

Samples	Fungal species	Numbers of grown isolates	Percentage (%) of grown isolates	Means
Sample 1	*Aspergillus fumigatus*	7.60	4.87	57.5%
	Aspergillus niger	17.90	11.08	
	Candida glabrata	17.98	11.17	
	Rhizopus oryzae	30.56	19.30	
	Mucor irregularis	19.89	12.01	
Sample 2	*Rhizopus oryzae*	16.80	10.07	20.9%
	Mucor sp.	17.33	10.77	
Sample 3	*Rhizopus oryzae*	18.93	12.00	21.5%
	Mucor irregularis	16.00	10	
Sample 4	*Aspergillus niger*	15.97	9.21	65.5%
	Rhizopus oryzae	20.00	11.66	
	Mucor irregularis	34.28	19.87	
	Candida glabrata	18.33	10.62	
	Aspergillus fumigatus	25.78	14.29	
Sample 5	*Aspergillus niger*	17.43	10.18	10.1%
	Mucor irregularis	16.83	10.42	24.4%
	Rhizopus oryzae	25.06	14.12	

Table 2. Fungal species related to COVID-19 infections

Fungal species in co-infection	Site/place	Country	Year	Author (s)
Aspergillus fumigatus	Pulmonary infection	Germany	2020	Koehler et al.[30]
Aspergillus fumigatus	Respiratory infection	EUA	2020	Mitaka et al.[31]
Candida glabrata *Aspergillus fumigatus*	Pulmonaryinfection/ Blood	China	2020	Lansbury et al.[32]
Candida glabrata	Blood	Colombia	2021	Frías-De-León et al.[33]
Rhizopus oryzae	Rhino-orbito-cerebral	Brazil	2021	Lacerda et al.[34]
Aspergillus fumigatus, A. niger	Pulmonary infection	Austria	2022	Lackner et al.[35]
Mucormycoses (black fungi)	Sino-nasal-orbital/ necroses	India	2022	Upadhayay et al.[36]

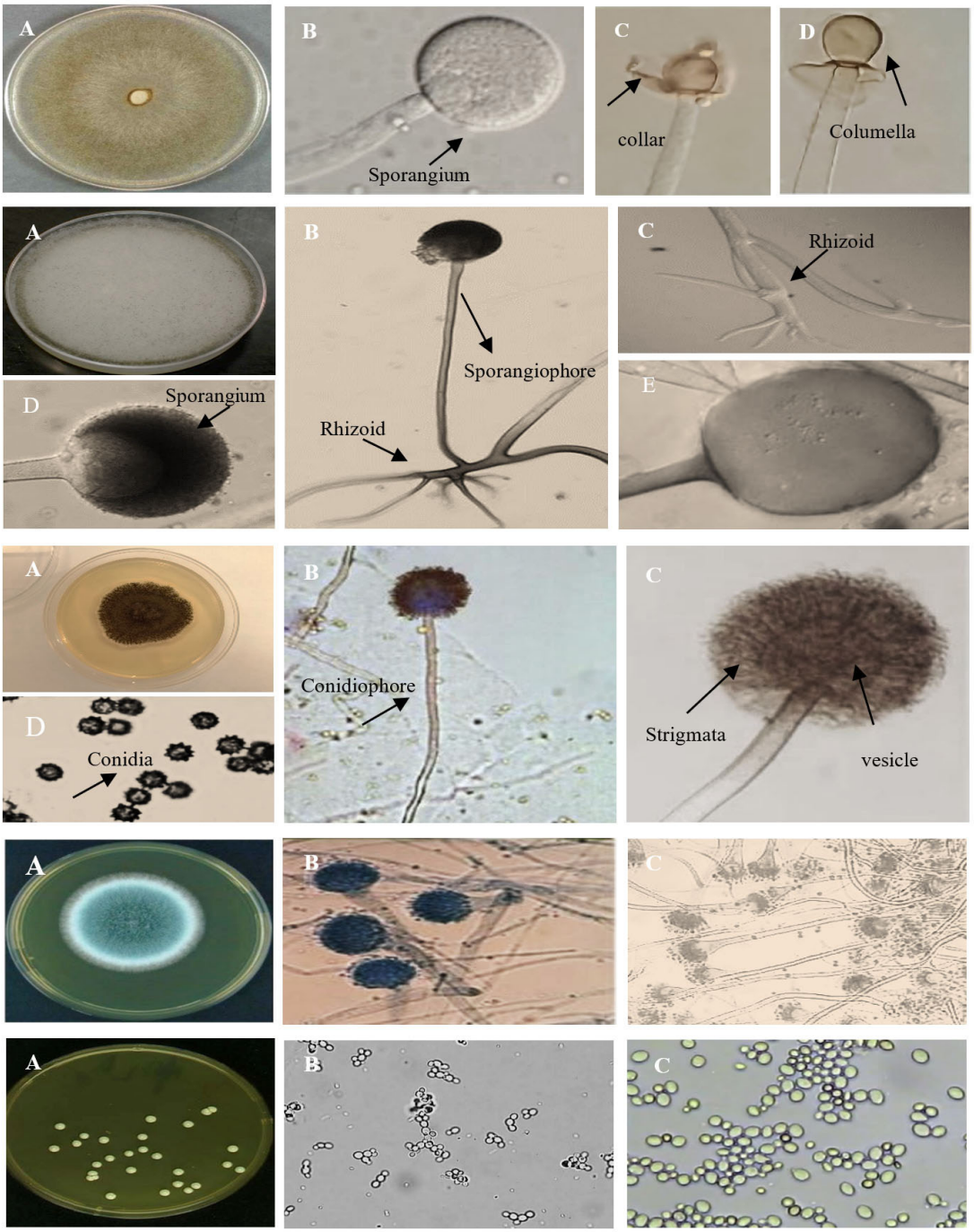

Figure 1. Morphological and microscopic characterization of isolated fungi. Microscopic photos of *Mucor irregularis* (A) on PDA medium, (B-D) Sporangiophores, sporangia, Sporangiospores and Columella with clear collar present (1). Microscopic photos of *Rhizopus oryzae* (A) on PDA medium, (B-E) Sporangiophores, Sporangia, Sporangiospores and Rhizoid present (2). Microscopic photos of *Aspergillus niger* (A) on PDA medium, (B-D) Conidia, conidiophore, vesicle present (3). Microscopic photos of *Aspergillus fumigatus* (A) on PDA medium, (B-C) Conidia, conidiophore, vesicle present (4). Microscopic photos of *Candida glabrata* (A) on PDA medium, (B-C) Budding yeast cells (5)

Characterization of the free ligand (L)$C_{20}H_{14}Br_2N_2O_2$ and its La-L-$(NO_3)_3C_{20}H_{14}Br_2N_5O_{11}$ nano complex

The displayed formula in Figure 2 is consistent with analytical findings of the used ligand in the current work. Analysis of C, H, N, and O has been investigated for both the ligand and it's La-nano-complex. The M.P. was sharp, displaying purity of the investigated compounds. In addition, the results of the elemental analysis of the produced complexes are in match with the requirements given by the complex's proposed formula.

The single peaks on 9.34 ppm & 11.25 ppm in NMR spectra of the free ligand (Figure 3) are attributed to the HC=N and OH protons, respectively. Also visible are multiple peaks

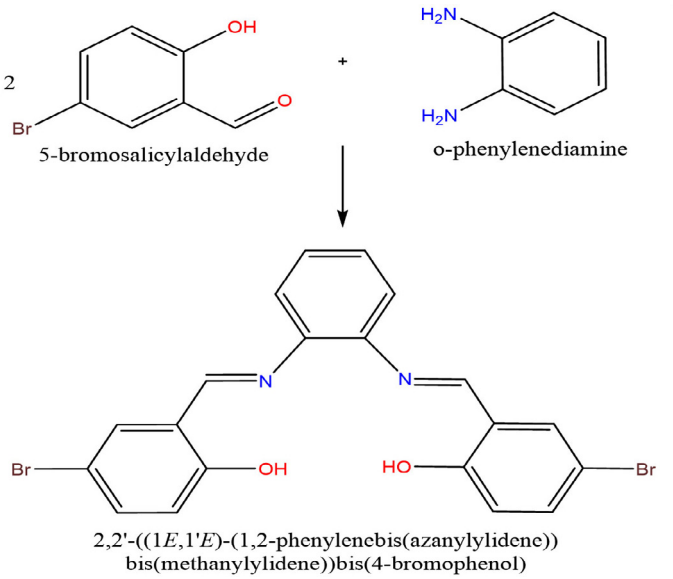

Figure 2. The proposed structure of the prepared free ligand

Table 3. Inhibition zones developed at different La-nano complex concentrations against isolated fungi

Fungal strain	Inhibition zone diameter (mm)				
	Control miconazole	0.32	0.64	1.28	2.56
Aspergillus fumigatus	13.4 ± 1.5	0	13.7 ± 1.8	17.9 ± 2.1	25 ± 0.8
Aspergillus niger	11.9 ± 0.01	0	15.9 ± 0.09	20.9 ± 0.8	28.7 ± 1.3
Candida glabrata	11.2 ± 2.02	0	15.2 ± 0.2	19.6 ± 1.00	28.6 ± 0.05
Mucor irregularis	12.1 ± 0.7	0	14.1 ± 1.4	18.3 ± 0.21	26.2 ± 0.13
Rhizopus oryzae	12.9 ± 1.7	0	15.5 ± 0.7	20.9 ± 1.13	27 ± 1.63

Table 4. Inhibition zones developed by coated filter with La-nano-complex at 0.64 mg/ml against isolated fungi

Fungal strain	Inhibition zone diameter (mm)			
	After 15 min	After 30 min	After 45 min	After 60 min
Aspergillus fumigatus	2.0 ± 2.01	3.2 ± 1.5	3.8 ± 0.09	5.1 ± 0.90
Aspergillus niger	2.8 ± 1.00	4.1 ± 0.5	4.6 ± 0.10	5.8 ± 0.01
Candida glabrata	2.5 ± 0.11	3.6 ± 1.7	4.0 ± 0.18	6.1 ± 0.08
Mucor irregularis	2.7 ± 0.06	3.5 ± 0.9	3.9 ± 2.00	4.8 ± 0.91
Rhizopus oryzae	2.5 ± 0.01	3.8 ± 1.2	4.2 ± 0.09	6.1 ± 0.21

representing aromatic protons between 6.4 and 8.18 ppm.[18,19] In contrast, the NMR data of the free Schiff base ligand and its La-nano complex are feasible to verify that the ligand and its metal ion have been complexed (Figure 4). The spectra of the La-nano complex show a noticeable shift in the signals attributable to the azomethine & phenolic protons after meticulous complexation. This observation implies that neutral tetradentate coordination via metal ions occurs without a need for deprotonation and both phenolic and azomethine groups are involved. The ligand also seems to act as an O_2N_2 coordination sphere.

To establish the type of bonding, the IR spectra of the free ligand and its nano complex were compared. The group of phenol (OH) is responsible for a great absorption band in the ligand's infrared spectra at 3456 cm^{-1}.[20,21] Due to the C-O (phenolic group), a medium band is also formed at 1290 cm^{-1} in the spectra. The azomethine group's C=N resulted in the formation of a strong band at 1620 cm^{-1}.[17] When the spectra of La complex were compared to that of the free ligand, the band at 3456 cm^{-1} altered to a lesser rate at 3400 cm^{-1}, demonstrating which OH group participated in complexation without being de-protonated. Strong bands associated with azomethine & C-O (azomethine & phenolic groups) at 1620 and 1290 cm^{-1} are stirred to lower wavenumbers (1530 cm^{-1} & 1250 cm^{-1}, respectively) in complex, indicating N & O coordination to the metal ion. Three additional spectral bands at 1400 cm^{-1}, 1370 cm^{-1}, and 1025 cm^{-1} that are displayed by the complex are all compatible with the coordination mode of the NO_3 group. The complete set of conductance

Table 5. Theoretical parameters of the ligand and its Lanthanum complex

	Ligand	La(III) complex
Binding Energy kcal/mol	-4695.16	-4949.05
E_{HOMO} (eV)	-5.11	-5.68
E_{LUMO} (eV)	-2.75	-3.60
Gap, "E	2.36	2.08
Ionization potential (eV)	5.11	5.68
Electron affinity	2.75	3.60
Absolute electronegativity	3.93	4.64
Absolute hardness	1.18	1.04
Chemical potential	-3.93	-4.64
Global softness	0.59	0.52
Global electrophilicity	6.54	10.35
Additional electronic charge	3.33	4.46
Dipole moment, (Debye)	2.85	2.25

Table 6. The Mulliken atomic charges of the ligand and its Lanthanum complex

Ligand				La(III) complex			
Atom	charge	Atom	charge	Atom	charge	Atom	charge
C (1)	0.031	C (2)	0.067	Br (1)	0.017	C (7)	-0.018
C (3)	0.352	O (4)	-0.493	C (2)	-0.026	O (8)	-0.425
C (5)	-0.098	C (6)	-0.043	C (3)	-0.019	O (9)	-0.407
C (7)	0.196	C (8)	-0.088	C (4)	-0.056	N (10)	0.728
N (9)	-0.292	Br (10)	-0.242	C (5)	0.312	O (11)	-0.406
C 11)	0.119	C (12)	0.124	C (6)	-0.067	O (12)	-0.281
C 13)	-0.068	C (14)	-0.046	C (35)	0.109	C (33)	0.152
C (15)	-0.047	C (16)	-0.065	N (34)	-0.255	C (32)	-0.051
C (17)	0.037	C (18)	0.059	C (31)	-0.041	C (30)	-0.034
C (19)	0.338	O (20)	-0.479	C (29)	-0.050	C (28)	0.147
C (21)	-0.086	C (22)	-0.044	N (27)	-0.254	C (26)	0.134
C (23)	0.184	C (24)	-0.076	O (25)	-0.409	O (24)	-0.282
N (25)	-0.283	Br (26)	-0.235	N (23)	0.739	O (22)	-0.400
				Br (21)	0.016	C (20)	-0.070
				C (19)	-0.024	C (18)	-0.032
				C (17)	-0.010	C (16)	-0.057
				C (15)	0.312	O (14)	-0.431
				La (13)	1.340		

data is supported by these findings. Novel bands in IR spectra of the metal nano complex in the low-frequency region at 545 cm^{-1} & 510 cm^{-1} may be assigned to these compounds because M-O & M-N, respectively, are not present in the spectrum of the free ligand, firmly proving bonding.[21,22]

The parent peak of the Schiff base ligand's mass spectrum is located in m/e = 474.36 (48.78%), which is the same as the chemical formula $C_{20}H_{14}Br_2N_2O_2$. The strength of the spectrum's many peaks, which stand for various fragments and indicate the stability of those parts,

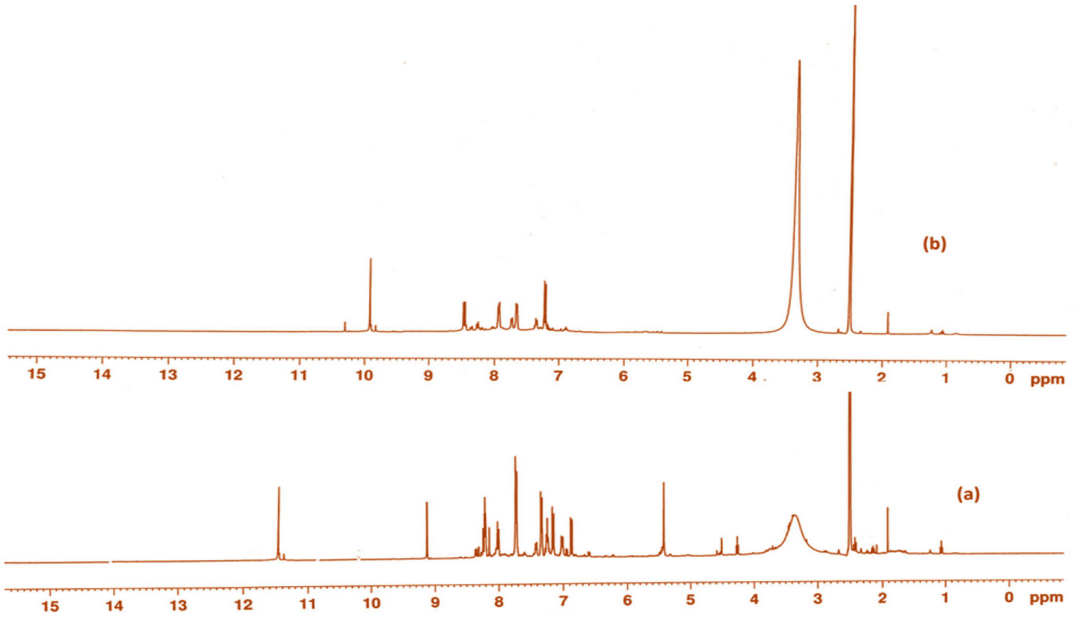

Figure 3. ^1H NMR data for (a) Free ligand and (b)

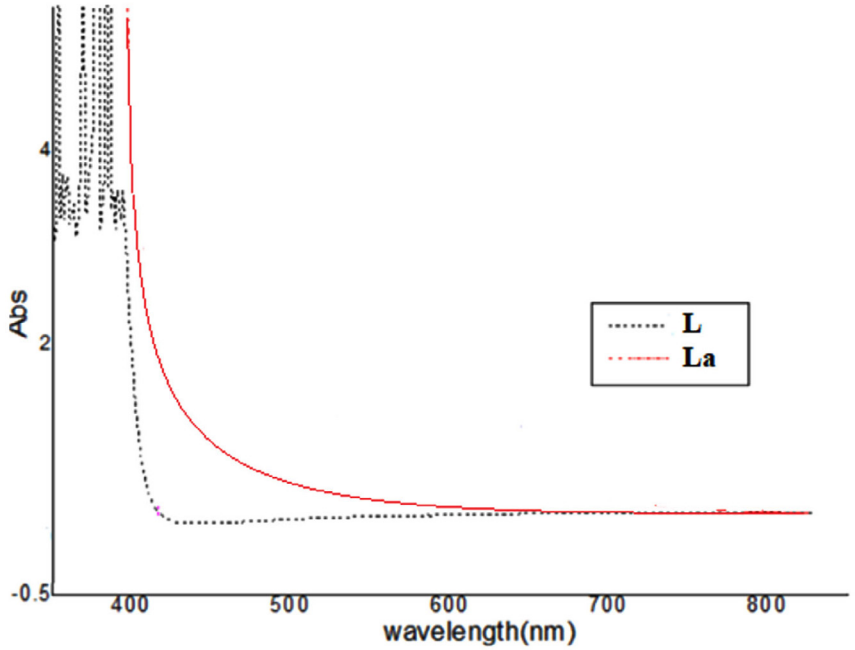

Figure 4. UV-vis spectra for the free ligand and its La complex

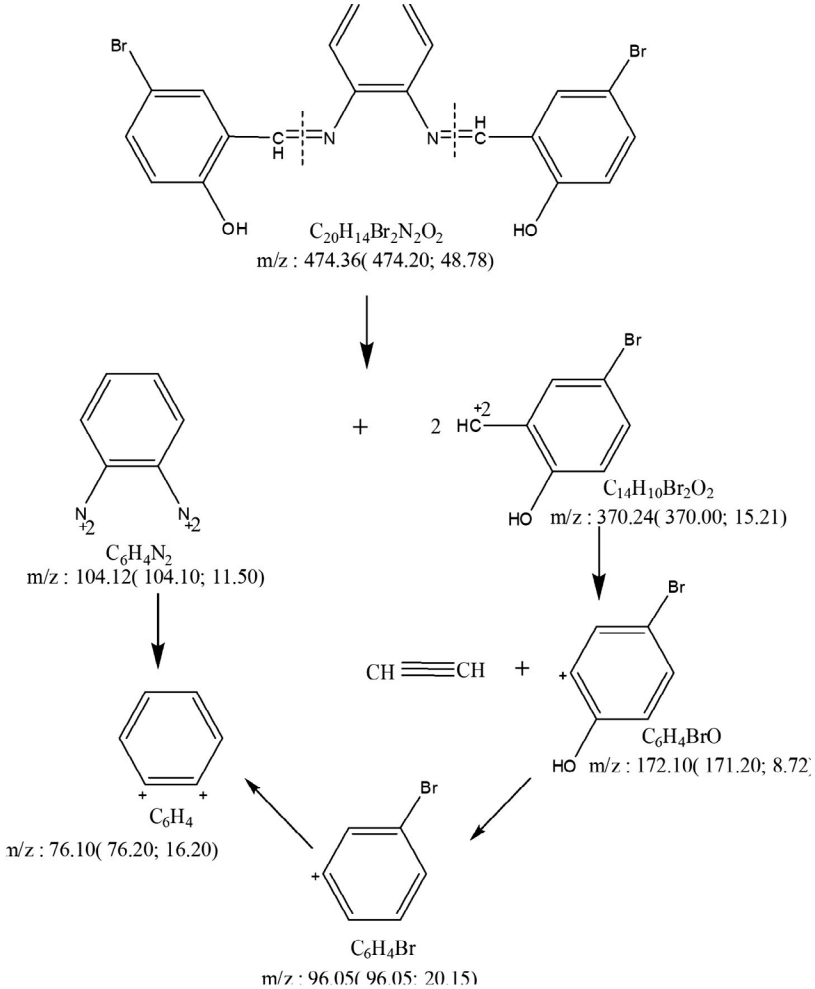

Figure 5. The pattern of mass fragmentation for the free ligand

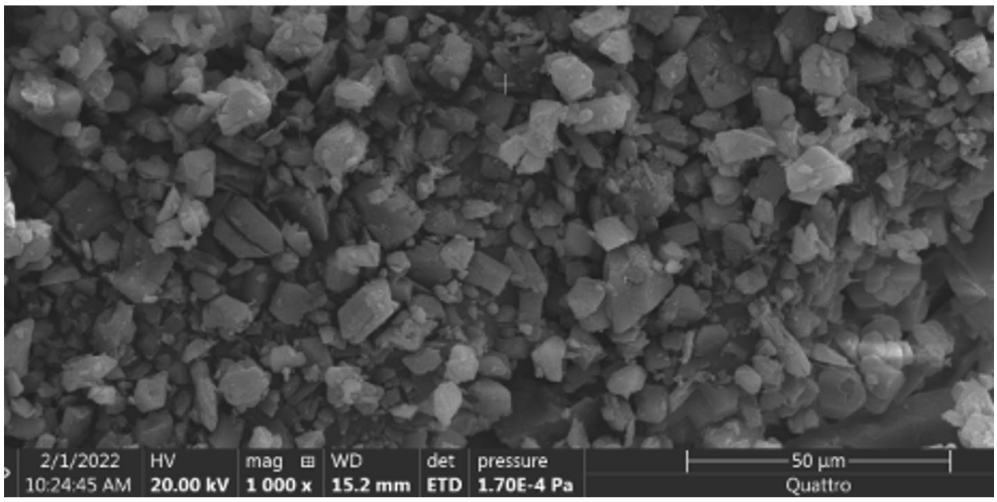

Figure 6. SEM image of nanoparticle complex

is another feature. The suggested mechanism for the decomposition phases of the ligand is depicted in Figure 5.

The conductivity value of the La-nano complex can be calculated using the formula m = K/C, where K is the specific conductance and

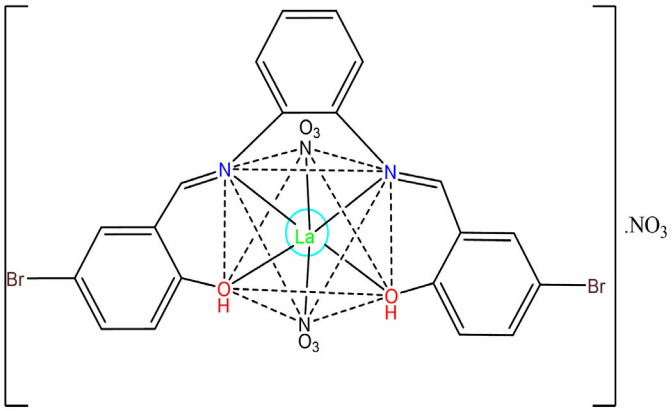

Figure 7. Expected structure of La nano complex

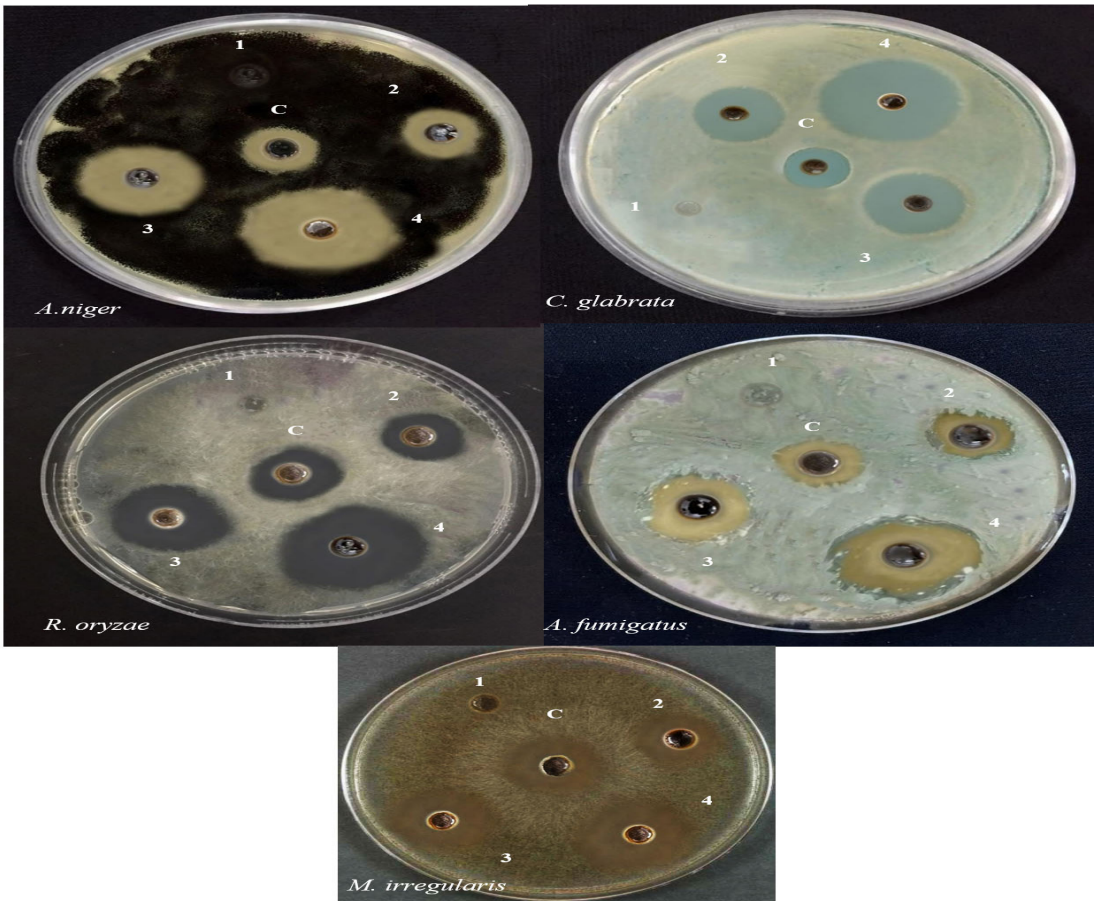

Figure 8. Effect of La-nano complex with different concentration, 0.32 mg/ml (1), 0.64 mg/ml (2), 1.28 mg/ml (3), and 2.56 mg/ml (4) on the growth of tested isolated fungi, under dark condition at 30°C

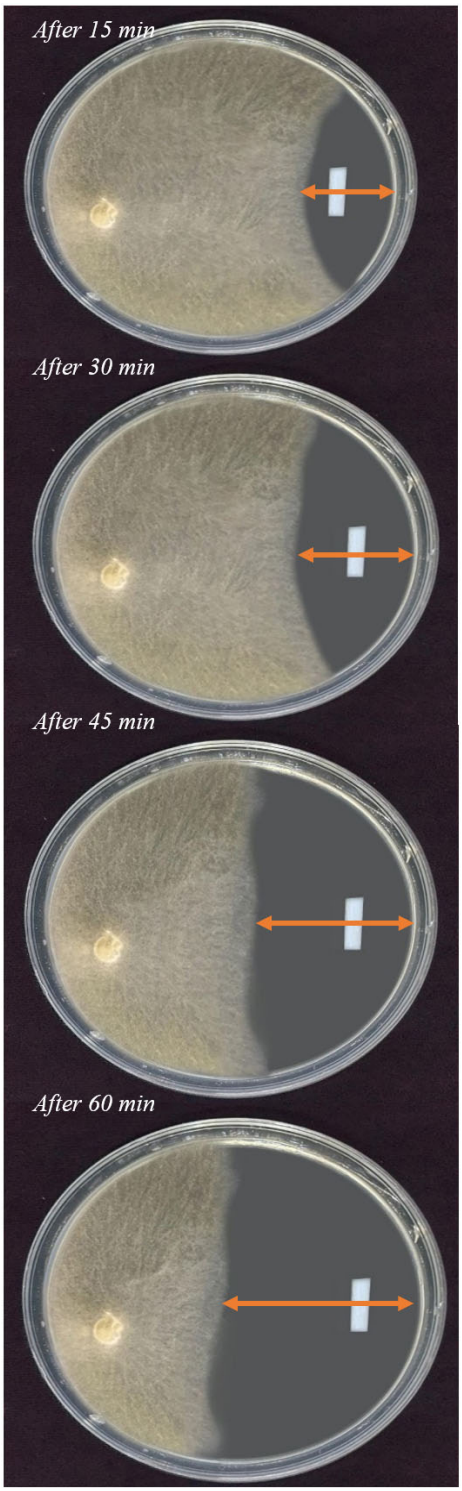

Figure 9. Effect of La-nano complex) 0.64 mg/ml) on the growth of *R. oryze*, under dark condition at 30°C, at different period

C is the molar concentration of the nanometal complex solution. Following the compound's dissolution in (10^{-3}M) DMF, the solution's molar conductivity was calculated at 25°C. According to the results, the complex has a molar conductance of 50.50 $Ohm^{-1}mol^{-1}cm^2$, which suggests that it is mono-electrolytic. Observations similarly show that nitrate ions are linked to metal cations.[21,23]

The Ultraviolet-vis spectra of the ligand & its metal complex in DMF were recorded at temperatures between 200 and 800 nm. Benzene & azomethine groups, respectively, were said to be responsible for two absorption peaks at 265 and 339 nm induced by π-π* and n-π* transitions in the ligand spectra.[20,22]

The coordination of the free ligand with the metal ion caused the bands related to π-π* and n-π* transitions in the spectrum of the e La nano complex to be shifted to a lower or higher frequency. No *d-d* transition exists in the La (III) complex. The octahedral structure may be suggested as a result of all of this knowledge.

SEM was used to investigate the size and shape of the nano complex (Figure 6). The particles seemed to be semi-spherical and/or Trapezoid in shape and to have some agglomerations. La(III) nanoparticles were stabilized by their interaction with the Schiff base ligand, as seen in SEM images.[24] The complex's structure can be inferred from the correlation of all these findings, as shown in Figure 7.

Antifungal activity

Limiting the growth of the mycelium of investigated fungi is considered the base of the antifungal activity in the current study. The results explored a concentration-dependent increase in biological activity, as indicated in Table 3,4 and Figure 8. The minimum inhibitory concentration (MIC) for the La-nano-complex was 0.64 mg/ml. Using an effective antifungal drug is crucial to save the patient's life which must be coupled with treating the underlying illness. When used to treat mucormycosis, the La-nano complex has shown promising effects in terms of reducing the activity of fungi.[37]

Effective control/treatment of COVID-19 and the other respiratory viruses like influenza requires wider insights to interfere/prevent

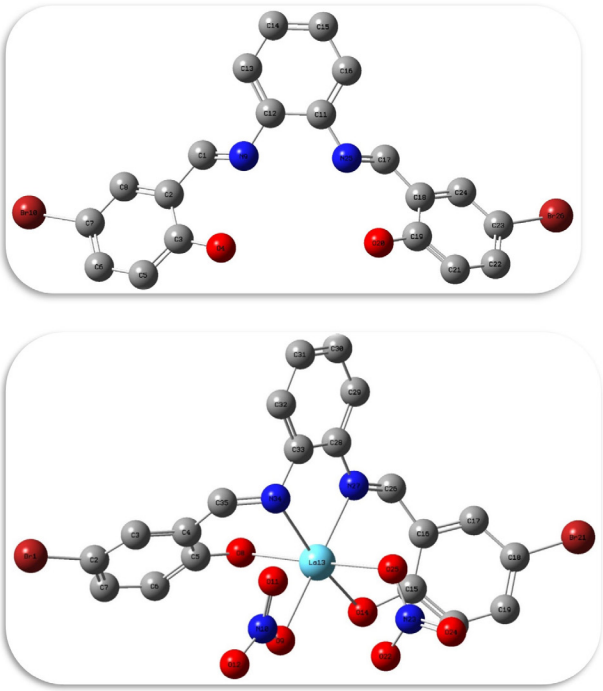

Figure 10. Optimized structure for Ligand and its La(III) complex with their labeling

planning for the prevention, diagnosis, and treatment of these infections.

The coated filter with La-nano-complex proved the ability of the compound at 0.64 mg/ml concentration to inhibit all isolated fungi when applied for 60 min with an inhibition rate of up to 95% (Table 4). In conclusion, we were able to isolate different fungal species from the filters of the air-conditioning systems in COVID-19 rehabilitation rooms which increase the risk of co-infections. However, the prepared La-nano-complex filters were able to significantly decrease the invading microbes and eradicate *Rhizopus, Aspergillus, Mucor, Candida albicans* isolates at 0.64 mg/ml concentration Figure 9.

DFT study

The optimized structure of the ligand and its Lanthanum complex with labeling of the atoms are presented in Figure 10.

Table 5 provides a comparison of various electronic properties between the ligand and its lanthanum complex. The ligand exhibits lower binding energy, ionization potential, electron affinity, absolute electronegativity, and chemical potential compared to the lanthanum complex. Meanwhile, the lanthanum complex displays smaller energy gap, absolute hardness, and global softness relative to the ligand. These findings indicate that coordination with lanthanum enhances molecular stability and electron-withdrawing nature. Specifically, the lanthanum complex features stronger bonding interactions, higher resistance to changes in electron density, and increased tendency to act as an electrophile in chemical reactions. Analysis of the HOMO-LUMO energy gap values observed reveals that the complex molecule possesses higher reactivity than the uncoordinated ligand molecule, as evidenced by its smaller energy gap ($\underline{E}$ = 2.08 eV for the complex, 2.36 eV for the ligand). This computational result corroborates well with the findings from biological activity assays, which demonstrated enhanced reactivity for the complex relative to the ligand alone. The decreased energy requirement for electron transition in the complex implies it may more readily undergo redox reactions involved in bioactivity mechanisms.

The atomic charges of the ligand and its Lanthanum complex as calculated by the Mulliken method[26] are presented in Table 6. Mulliken charges have a direct correlation with a molecule's vibrational properties. The distribution of positive and negative charges among atoms is a primary factor influencing increases or decreases in bond lengths. Specifically, polarization of charge away from bonding atomic centers tends to elongate bonds by weakening orbital overlap, while accumulation of charge between atoms serves to strengthen interactions and shorten distances. Computational analysis of Mulliken charges can provide useful insights into how coordination and charge transfer may impact fundamental vibrational characteristics by altering electrostatic forces along chemical bonds at the atomic scale. Higher electrophilic charge density is observed on the oxygen and nitrogen atoms. Notably, the charge on the N and o atoms atom in the ligand are more negative than other atoms, indicating that they have greater ability for metal ion coordination due to increased basicity.[27] Upon complexation, the electrophilic charge densities increase relative to the uncoordinated ligand. This trend correlates well with the higher biological activity observed experimentally for the cobalt complex versus the ligand alone. The increased charge polarization upon complexation implies stronger binding interactions with biological targets, enhancing reactivity profiles in accordance with observed bioactivity outcomes.

CONCLUSION

Fungal co-infections are identified from air conditioning filters in the rooms of critically sick COVID-19 patients, with aspergillosis having the highest incidence, followed by candidemia. In light of these connections between fungi and infections, as well as between some treatments and fungi, contemporary medical practices are challenged to come up with creative ways to prevent subsequent fungus infections. The prognosis for COVID-19 patients may be improved in the interim, nevertheless, by quick detection of fungus co-infections and treatment with antifungal medication. The lanthanum complex exhibits enhanced stability and electron-withdrawing nature, as evidenced by its lower binding energy, ionization potential, electron affinity, absolute electronegativity, and chemical potential. Additionally, the lanthanum complex displays a smaller energy gap, absolute hardness, and global softness, indicating optimized structural features and reactivity profiles.

ACKNOWLEDGMENTS

The authors would like to thank the Deputyship for Research and Innovation, Ministry of Education in Saudi Arabia, for funding this research work through project number DSR-2021-03-03127.

CONFLICT OF INTEREST

The authors declare that there is no conflict of interest.

AUTHORS' CONTRIBUTION

SMNM, RHT conceptualized and visualized the study. SMNM, RHT applied methodology. SMNM, TAY and RHT performed experiments. SMNM, TAY, RHT performed data curation. SMNM, TAY and RHT performed data analysis. SMNM, TAY and RHT drafted the manuscript. SMNM, TAY and RHT wrote the manuscript. SMNM and RHT reviewed the manuscript. All authors read and approved the final manuscript for publication.

FUNDING

This study was supported by the Deanship of Scientific Research at Jouf University through research grant No. (DSR-2021-03-03127).

DATA AVAILABILITY

The datasets generated and/or analysed during the current study are available from the corresponding author on reasonable request.

ETHICS STATEMENT

This article does not contain any studies on human participants or animals performed by any of the authors.

REFERENCES

1. Pal M. Zygomycosis: A highly infectious emerging opportunistic fungal disease of public health concern. *OAJMMS.* 2020;3(1):000122. doi: 10.23880/OAJMMS-16000122
2. Pal M, Lee CW. Pulmonary zygomycosis in chicks

due to Absidia corymbifera. *Korean J Vet Clin Med.* 1994;11(1):339-341.
3. Pal M. Veterinary and Medical Mycology. 1st (Edn.), ICAR, New Delhi, India. 2007.
4. Eucker J, Sezer O, Graf B, Possinger K. Mucormycoses. *Mycoses.* 2001;44(7):253-260. doi: 10.1111/j.1439-0507.2001.00656.x
5. Raut A, Huy NT. Rising incidence of mucormycosis in patients with COVID-19: another challenge for India amidst the second wave. *Lancet Respir Med.* 2021;9(8):e77.doi: 10.1016/S2213-2600(21)00265-4
6. Sugar AM. Mucormycosis. *Clin Infect Dis.* 1992;14(1):126-129. doi: 10.1093/clinids/14.Supplement_1.S126
7. Chayakulkeeree M, Ghannoum MA, Perfect JR. Zygomycosis: the re-emerging fungal infection. *Eur J Clin Microbiol Infect Dis.* 2006;25(4):215-229. doi: 10.1007/s10096-006-0107-1
8. Mantadakis E, Samonis G. Clinical presentation of zygomycosis. *Clin Microbiol Infect.* 2009;15(S5):15-20. doi: 10.1111/j.1469-0691.2009.02974.x
9. Singh AK, Singh R, Joshi SR, Mishra A. Mucormycosis in COVID-19: A systematic review of cases reported worldwide and in India. *Diabetes Metab Syndr.* 2021;15(4):102146.doi: 10.1016/j.dsx.2021.05.019
10. Centers for Disease Control and Prevention Fungal diseases. 2019. https://www.cdc.gov/fungal/diseases/mucormycosis/risk-prevention.html
11. Sutherland Ken. 5th ed. Filters and Filtration Handbook. *Elsevier.* 2008. doi: 10.1016/B978-1-85617-464-0.00004-3
12. Araujo R, Cabral JP. Fungal air quality in medical protected environments. *Air Qual.* 2010. doi: 10.5772/9766
13. Deshmukh SP, Patil SM, Mullani SB, Delekar SD. Silver nanoparticles as an effective disinfectant: A review. *Mater Sci Eng C Mater Biol Appl*. 2019;97:954-965. doi: 10.1016/j.msec.2018.12.102
14. Balagna C, Francese R, Perero S, Lembo D, Ferraris M. Nanostructured composite coating endowed with antiviral activity against human respiratory viruses deposited on fibre-based air filters. *Surf Coat Technol.* 2021;409:126873. doi: 10.1016/j.surfcoat.2021.126873
15. Park K, Kang S, Park J-W, Hwang J. Fabrication of silver nanowire coated fibrous air filter medium via a two-step process of electrospinning and electrospray for anti-bioaerosol treatment. *J Hazard Mater*. 2021;411:125043. doi: 10.1016/j.jhazmat.2021.125043
16. Ju Y, Han T, Yin J, et al. Bumpy structured nanofibrous membrane as a highly efficient air filter with antibacterial and antiviral property. *Sci Total Environ*. 2021;777:145768. doi: 10.1016/j.scitotenv.2021.145768
17. Taha RH. Preparation, Spectroscopic Characterization, DNA Cleavage, Antimicrobial and Antitumor Investigations of Nickel and Uranyl Schiff Base Complexes in Bulk and Nano size. *Curr Sci Int*. 2015;4(4):684-700.
18. Fasina TM, Ogundele OO, Ayeni I. Synthesis and biological properties of N_2O_2 Schiff bases derived from o-phenylenediamine and substituted salicylaldehydes. *J Chem Pharm Res.* 2014;6(6):816-819.
19. Taha RH, Almutlq NJ, Elnasr TAS, Alshammari MS, Mohamed SH, Moustafa SM. Ce and Fe complexes as potent antifungal agents for wallpapers. *Bull. Chem. Soc. Ethiop*, 2024; 38(2), 365-383. doi: 10.4314/bcse.v38i2.7
20. Moustafa SMN, Taha RH. Mycogenic Nano-Complex for Plant Growth Promotion and Bio-Control of *Pythium aphanidermatumm*. *Plants.* 2021;10(9):1858. doi: 10.3390/plants10091858
21. Gomathi V, Selvameena R. Synthesis, Physico chemical and Antimicrobial Studies on Schiff Base Complexes of Sulfa Drug with Metals of Life. *Indian J Appl Res.* 2013;3(4):51-53.
22. Karekal MR, Biradar V, Mathada MBH. Synthesis, Characterization, Antimicrobial, DNA Cleavage, and Antioxidant Studies of Some Metal Complexes Derived from Schiff Base Containing Indole and Quinoline Moieties. *Bioinorg Chem Appl.* 2013;2013:315972.doi: 10.1155/2013/315972
23. Alsohaimi IH, Alotaibi NF, Albarkani AM, et al. Photocatalytic wastewater treatment and disinfection using green ZnO-NP synthesized via cera alba extract. *Alexandria Engineering Journal,* 2023;83, 113-121. doi: 10.1016/j.aej.2023.10.037
24. Moustafa SMN, Taha RH. Biosynthesis of Zinc Nanocomplex Employing for Plant Growth Promotion and Bio-Control of *Pythium ultimum.* Intechopen. 2021. doi: 10.5772/intechopen.100185
25. Taha RH, Alrabie A, Badr EE, Shymaa MN, Baker SA. Design, synthesis, characterization, spectral, chemical analysis, biological evaluation, and molecular docking studies of novel fatty Schiff base ligands and their nickel and mercury complexes. *Inorganic Chemistry Communications,* 2023;158:111382. doi: 10.1016/j.inoche.2023.111382
26. Ahmed RM, Yousif EI, Hasan HA, Al-Jeboori MJ. Metal Complexes of Macrocyclic Schiff-Base Ligand: Preparation, Characterisation, and Biological Activity. *ScientificWorldJournal*. 2013;2013:289805. doi: 10.1155/2013/289805
27. Wu X, Ray AK. Density-functional study of water adsorption on the PuO 2 (110) surface. *Physical Review B.* 2002;65(8):085403. doi: 10.1103/PhysRevB.65.085403
28. Mohamed GG, Zayed MA, Abdallah SM. Metal Complexes of a Novel Schiff Base Derived from Sulphametrole and Varelaldehyde. Synthesis, Spectral, Thermal Characterization and Biological Activity. *J Mol Struct.* 2010;979(1-3):62-71. doi: 10.1016/j.molstruc.2010.06.002
29. Seyedjavadi SS, Bagheri P, Nasiri MJ, Razzaghi-Abyaneh M, Goudarzi M. Fungal infection in co-infected patients with COVID-19: an overview of case reports/case series and systematic review. *Front. Microbiol*. 2022;13:888452
30. Mandegani Z, Mozaffar A, Zahra A, Afshan M, Nasser I, Akbar O. A Nano Tetraimine Pd(0) Complex: Synthesis, Characterization, Computational Studies and Catalytic Applications in the Heck-Mizoroki Reaction in Water. *Green Chem.* 2015;17:3326-3337. doi: 10.1039/

C5GC00616C

31. Koehler P, Cornely OA, Böttiger BW, et al. COVID-19 associated pulmonary aspergillosis. *Mycoses*, 2020; 63(6):528-534. doi: 10.1111/myc.13096
32. Mitaka H, Perlman DC, Javaid W, Salomon N. Putative invasive pulmonary aspergillosis in critically ill patients with COVID-19: an observational study from New York City. *Mycoses*, 2020;63(12):1368-1372. doi: 10.1111/myc.13185
33. Lansbury L, Lim B, Baskaran V, Lim WS. Co-infections in people with COVID-19: a systematic review and meta-analysis. *Journal of infection*, 2020;81(2):266-275. doi: 10.1016/j.jinf.2020.05.046
34. Frías-De-León MG, Hernández-Castro R, Conde-Cuevas E, et al. Candida glabrata antifungal resistance and virulence factors, a perfect pathogenic combination. *Pharmaceutics,* 2021;13(10):1529. doi: 10.3390/pharmaceutics13101529
35. Bonates P, João GAP, Cruz KS, et al. Fatal rhino-orbito-cerebral mucormycosis infection associated with diabetic ketoacidosis post-COVID-19. *Rev Soc Bras Med Trop.* 2021;54:e03582021. doi: 10.1590/0037-8682-0358-2021.
36. Lackner N, Thomé C, Öfner D, et al. COVID-19 associated pulmonary aspergillosis: diagnostic performance, fungal epidemiology and antifungal susceptibility. *J. Fungi*. 2022;8(2):93. doi: 10.3390/jof8020093
37. Upadhayay P, Bansal K, Goyal A. Epidemiology, Risk Factors, Diagnosis and Treatment of Mucormycosis (Black Fungus): A Review. *Current Pharmaceutical Biotechnology,* 2023;24(13):1645-1656. doi: 10.2174/1389201024666230320111644